Smart Structures and Systems, *Vol. 21, No. 6 (2018) 751-759*
DOI: https://doi.org/10.12989/sss.2018.21.6.751

Localisation of embedded water drop in glass composite using THz spectroscopy

Magdalena Mieloszyk[*1], Katarzyna Majewska[1a] and Wieslaw Ostachowicz[1,2b]

[1]*Department of Mechanics of Intelligent Structures, Institute of Fluid Flow Machinery, Polish Academy of Sciences, 14 Fiszera Str., 80-231 Gdansk, Poland*
[2]*Faculty of Automotive and Construction Machinery Engineering, Warsaw University of Technology, 84 Narbutta Str., 02-524 Warsaw, Poland*

(Received May 20, 2017, Revised November 18, 2017, Accepted November 28, 2017)

Abstract. Glass fibre reinforced polymers (GFRP) are widely exploited in many industrial branches. Due to this Structural Health Monitoring systems containing embedded fibre optics sensors are applied. One of the problems that can influence on composite element durability is water contamination that can be introduced into material structure during manufacturing. Such inclusion can be a damage origin significantly decreasing mechanical properties of an element. A non-destructive method that can be applied for inspection of an internal structure of elements is THz spectroscopy. It can be used for identifications of material discontinuities that results in changes of absorption, refractive index or scattering of propagating THz waves. The limitations of THz propagation through water makes this technique a promising solution for detection of a water inclusion. The paper presents an application of THz spectroscopy for detection and localisation of a water drop inclusion embedded in a GFRP material between two fibre optics with fibre Bragg grating sensors. The proposed filtering method allowed to determine a 3D shape of the water drop.

Keywords: THz spectroscopy; glass fibre composite; fibre optics; moisture

1. Introduction

Composite structures are widely exploited in many industrial branches like aviation (Hajrya and Mechbal 2015), marine (Wang *et al.* 2001) or civil engineering (Alizadeh and Dehestani 2015). Due to wide applicability composite materials are exposed to different environmental and loading conditions. To increase the safety different Structural Health Monitoring (SHM) methods and Non-Destructive Techniques (NDT) are developed.

The high safety requirements results in SHM systems contains many sensors permanently installed on many civil engineering structures like bridges (Wang *et al.* 2016, Miyamoto and Motoshita 2017, Li *et al.* 2015, Zhou *et al.* 2013), wind turbines (Lecheb *et al.* 2015, Fifo *et al.* 2015), buildings (Xu *et al.* 2015, Teng *et al.* 2015) or offshore structures (Jung *et al.* 2015). SHM can serve as a tool to develop the methods of life-cycle performance design, evaluation, maintenance and management of structures. The feedback from SHM results allows to better understanding the element's behaviour under natural or man-made loadings/ influences (Li *et al.* 2015). The systems based on sensors installed on the structures' surfaces or embedded into material of particular elements. Among many techniques those based on fibre optics sensors (both distributed and fibre Bragg grating (FBG)) are popular. They are applied for measurement of strain, temperature or used in vibration based methods. Ciminello *et al.* (2015) developed an original SHM system based on FBG sensors for the strain monitoring of an adaptive wing element. Sung *et al.* (2017) designed a special tendon with embedded FBG sensors. It was applied for long-term SHM of tensile forces on a ground anchor of a bridge. Zhang *et al.* (2016) analysed optimal strain long-gauge fibre optic sensor layout on the tied arch bridge. Malekzadeh *et al.* (2014) presented four-span bridge model equipped with FBG sensors array as a part of SHM system.

Among many composite materials Glass Fibre Reinforced Polymers (GFRP) are recently very popular and find various applications. Due to this their behaviour under different loading and environmental factors are investigated. Ansari and Chakrabartia (2016) presented experimental and numerical analysis of GFRP plates with different thickens under ballistic impact with varying projectile nose shapes and incidence velocities. Xin *et al.* (2015) experimentally and theoretically investigated the coefficients of thermal expansion of GFRP laminates with different lamina stacking-sequence. The achieved results were applied for analysis of the thermal behaviours of composite girder with hybrid GFRP-concrete deck. Numan *et al.* (2016) analysed the behaviour of composite box girder bridges subjected to environmental factors: solar radiation, atmospheric temperature, and wind speed.

*Corresponding author, Ph.D.
E-mail: mmieloszyk@imp.gda.pl
[a] Ph.D.
E-mail: k.majewska@imp.gda.pl
[b] Professor
E-mail: wieslaw@imp.gda.pl

ISSN: 1738-1584 (Print), 1738-1991 (Online)

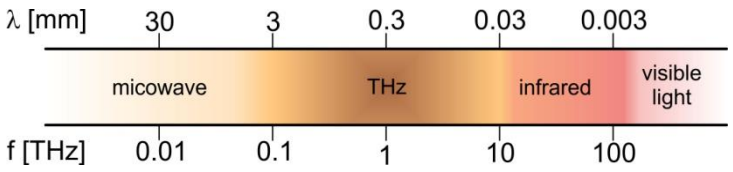

Fig. 1 Electromagnetic waves range (Mieloszyk *et al.* 2017)

(Lecheb *et al.* (2015) analysed evolution of a fatigue crack in a GFRP 25 m length wind turbine blade. Kim *et al.* (2017) designed FBG sensor for monitoring of cyclic thermal loading especially for railways applications. Park *et al.* (2016) developed an innovative GFRP/steel hybrid bar for stronger durability of concrete structures. Fifo *et al.* (2015) presented a novel concept of self-healing of GFRP wind turbine blades. In the present solution the repairing fluids were delivered to damaged sites by multiple hollow channels created within the composite, inherently in the polymeric matrix at fabrication.

Among many environmental factors (moisture, temperature, ultraviolet radiation, etc.) that can affect the durability of composite structures moisture is one of the most important (Budhe *et al.* 2017). The moisture affects a polymer properties, like dimensional stability, mechanical, chemical (Chaichanawong *et al.* 2016) and thermophysical properties (Eftekhari and Fatemi 2016).

Because GFRP elements are also joined to concrete parts of structures the moisture can diffuse also throughout concrete elements. Zhang *et al.* (2015) investigated numerically moisture transport in concrete in atmospheric environment during both wetting and drying process. In the study both the thickness of the adsorbed layer, the pore-size distribution were taken into consideration. Sarkar and Bhatacharjee (2014) proposed a numerical method for analysing the evolution of moisture distribution in concrete subjected to wetting-drying exposure caused by intermittent periods of rainfall. During the analysis also the influence of various meteorological factors. Rain, wind, relative humidity, temperature were taken into consideration. Beldjelili *et al.* (2016) analysed the hygro-thermo-mechanical bending behaviour of sigmoid functionally graded material plate resting on variable two-parameter elastic foundations.

The most typical moisture sources are presented in Table 1. Due to different localisation (internal or external) they were divided into two main groups: manufacturing and post-manufacturing. In the first case a drop of water that is introduced into laminate structure during manufacturing process is permanently trapped by surrounded epoxy resin. Such water cannot be removed and can negatively influenced on element's durability being an origin of different damage types like delamination or crack. In the second case the diffusion processes are the most important ones and they determine time and depth of the swelling process influence. Due to high absorption properties of polymers composite elements are protected against post-manufacturing sources of moisture by appropriate covers or painting layers.

Table 1 Moisture sources

Manufacturing	Post-manufacturing
Malfunction of production line	Normal exploitation
Human fault	Environment
	Accident or catastrophe

The strong influence of moisture on composite materials internal structure results in development of different NDT to detect and localise moist areas in elements. It is also important to determine size of water drop embedded into material during manufacturing process. The internal structure of a composite element can be inspected using different techniques based on electromagnetic radiation. Its spectral range is divided into several ranges (Fig. 1) based on interaction between wave and material structure. Due to this the wave ranges are related to NDT methods like infrared thermography or THz spectroscopy.

THz spectroscopy technique can be applied for inspection of internal structure of non-conductive materials like GFRP composites or polymers. It cannot be applied for metals because in the case whole signal is totally reflected from element's surface (Chan *et al.* 2007). Due to the fact that the power generated by THz beam is very low so risk of destroying sensitive materials is strongly limited (Cai *et al.* 1997). THz radiation can be used in analysis of materials that affects minimum one of three THz wave parameters: refractive index, absorption coefficient or wave scattering (Mittleman 2003). For GFRP elements the THz technique can be applied for identification of defects like: gaps, delaminations (Ryu *et al.* 2016), mechanical damage (Dong *et al.* 2016), burning on a material surface (Balbekin *et al.* 2015) or thermal degradation (Radzienski *et al.* 2015).

Water is highly absorptive in the THz range, while most materials which absorb moisture are either very transparent (e.g. paper, epoxy) or reasonably transparent to THz wave (Baldacci *et al.* 2017). One of the application is demonstration of THz imaging of moisture distribution of a drying leaf (Federici 2012).

The THz spectroscopy was also applied for detection and localisation of the water layer with thickness 100 – 300 μm in a joint between two GFRP elements (Malinowski *et al.* 2015). The relatively high permittivity of liquid water compared to GFRP material in the THz range enables a contrast mechanism for the detection and imaging of moisture. Three images (A-scan , B-scan and C-scan) of the analysed element are presented in Fig. 2. In signals presented in A-scan and B-scan (for the area with water occurrence) the THz wave is attenuated results in lack of reflection from the bottom boundary of the joint. The wet area shape is visible on C-scan.

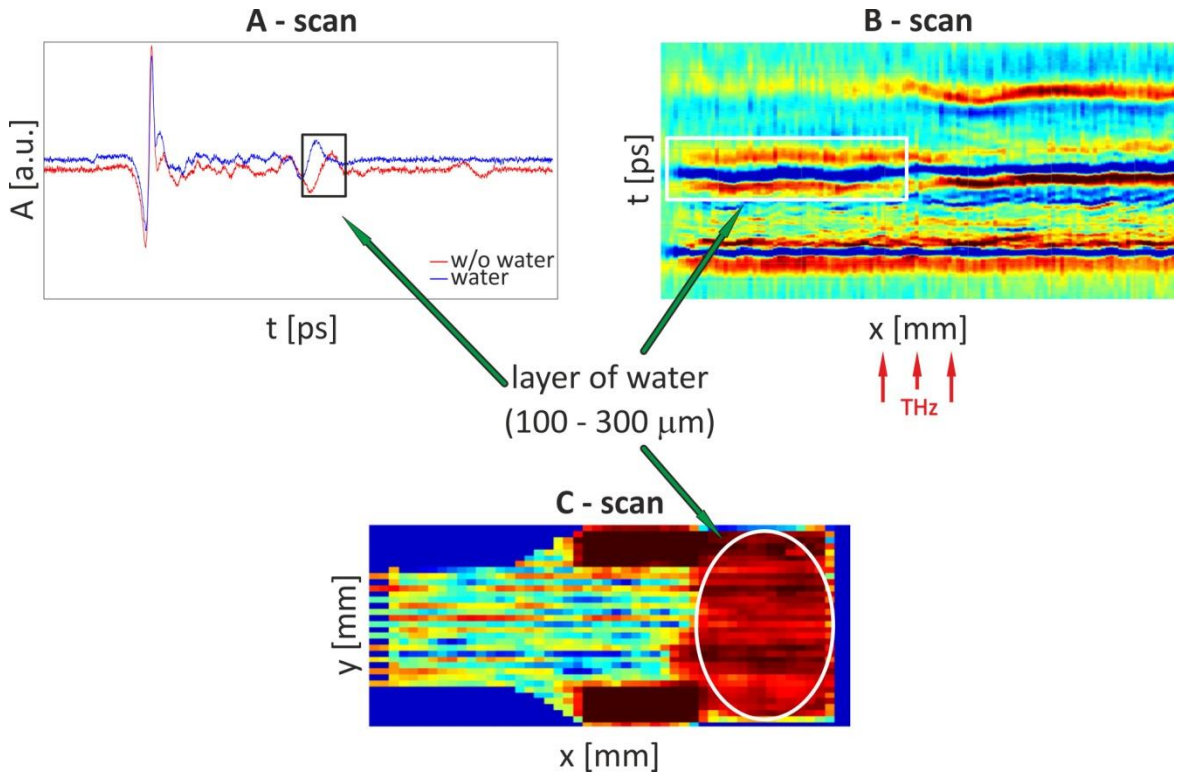

Fig. 2 Sample with water layer with thickness 100 – 300 µm (based on Malinowski *et al.* 2015)

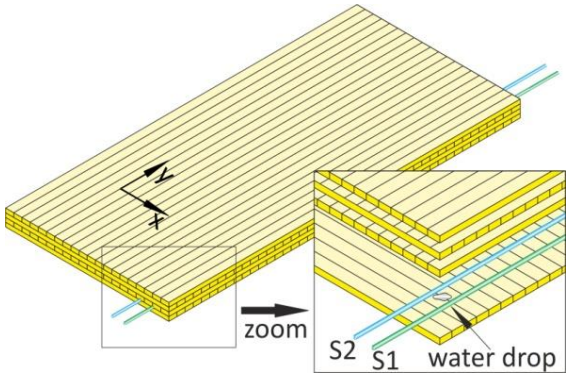

Fig. 3 Schema of the sample with water drop inclusion with denoted axis of THz spectrometer

The successful applications of THz spectroscopy for detection of moisture in different materials/ structures were a motivation for applying this technique for detection and imaging of moisture in a form of a water drop inclusion in GFRP laminate. The experimental investigation presented in the paper was performed on four-layered rectangular GFRP sample manufactured using infusion method. The THz spectroscopy was applied for observation and evaluation of the internal structure of the sample.

The paper is organised as follow. Firstly measurement set-up and GFRP sample with water drop inclusion are described. Then the experimental investigation results are presented and discussed. Finally some conclusions are drawn.

2. Experimental investigation

The measurements were performed on four-layered rectangular GFRP sample with a dimension of 70 mm x 200 mm x 1.6 mm. The laminate was manufactured using infusion method for bidirectional material (glass SGlass®) and epoxy resin. Between 1st and 2nd layer counting form the bottom of the sample two fibre optic with FBG sensors were embedded. Between them a water drop was introduced that was surrounded by epoxy resin during the manufacturing process and permanently trapped when the curing process was finished – Fig. 3.

The sample was previously examined using another NDT method in electromagnetic wave range (Fig. 1) – active infrared thermography (vibro- and pulse). It allowed to determine the location and size of the water drop

inclusion. Although limitations of the thermography method did not allow to determine the thickness of the inclusion and its exact location between layers. The detailed description of this investigation is presented in Majewska *et al.* (2016).

The internal structure of the sample was examined using THz spectrometer (TPS Spectra 300 THz Pulsed Imaging and Spectroscopy from TerraView®) in reflection mode. The measuring heads were arranged in a angle of 22℃ between them. The system contains scanning unit (Gantry Imaging System) with moving platform that allows to scanning chosen area of samples. During scanning process of the investigated sample the measurement step was equal to 0.2 mm and THz signals were registered with 10 averaging. As the THz waves are sensitive on moisture in the ambient all measurements were performed with air dryer that removes moisture from the working heads area and air condition that stabilise laboratory temperature on assumed level equal to 20℃.

3. Experimental results

A part of the sample with water inclusion was scanned by THz spectrometer. The preliminary results were presented in Mieloszyk *et al.* (2017). Comparison of frequency spectra and waveforms for material without and with water inclusion are presented in Figs. 4 and 5, respectively. As it is visible in the graph (Fig. 4) the frequency spectra are similar despite water occurrence. It is probably due to the fact that the amount of water is small so THz waves propagates throughout this area travelled mostly by the GFRP material. For both cases the highest amplitudes are achieved for the same frequencies equal to 0.5 THz. This information was used for comparison of material parameters of analysed water and GFRP in THz range. As it is visible in the graph (Fig. 4) for the 90% of energy is achieved for frequencies up to 2 THz. This information was used to remove the noise – for all signals the frequencies higher than 2 THz were filtered.

A comparison of two filtered and normalised signals for material without/ with water are presented in Fig. 5. The water influence is visible as attenuation of a maximum (reflection from the 2nd layer). It is denoted by 'W' and blue ellipse in the graph (Fig. 5(a)). This part is presented separately in Fig. 5(b) as a zoomed image focused on water influenced region. On contrary to the water layer in joint presented previously the embedded water influence is very local and is observable in this location only. This effect for the next layers of the sample is neglected. In the case THz waves propagate throughout mix of glass fibres, epoxy resin and water. Due to this it is harder to determine the water drop location and size than water layer. During the manufacturing process water was introduced between two layers so its thickness is comparable to the epoxy layer thickness between them.

To compare behaviour of water and GFRP in THz wave range their material parameters (absorption coefficient (κ) and refractive index (*n*) are analysed.

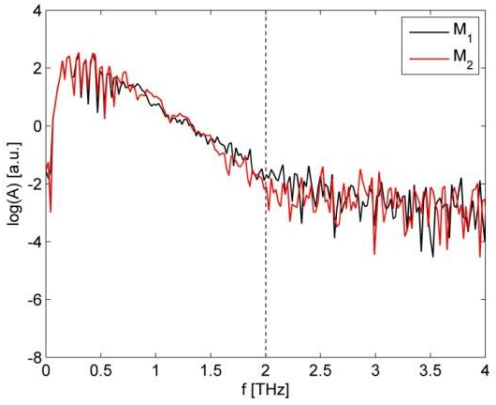

Fig. 4 A comparison of frequency spectra for intact (M_1) material and with the water inclusion (M_2)

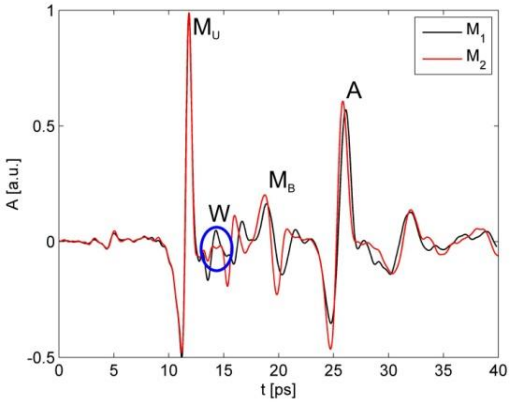

(a) Whole measured time

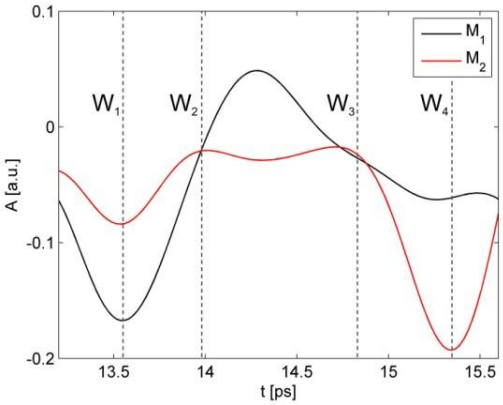

(b) Zoom focused on the water influenced region

Fig. 5 A comparison of waveforms for intact (M_1) material and with the water inclusion (M_2); M_U, M_B - reflections from upper and bottom surfaces of the sample, A - reflection from the metal table, W - water influence

The parameters are determined experimentally for a range of frequencies and their values are frequency dependent. Due to this the comparison was performed for one chosen frequency value equal to 0.5 THz related to maximum amplitude in frequency spectrum of GFRP material.

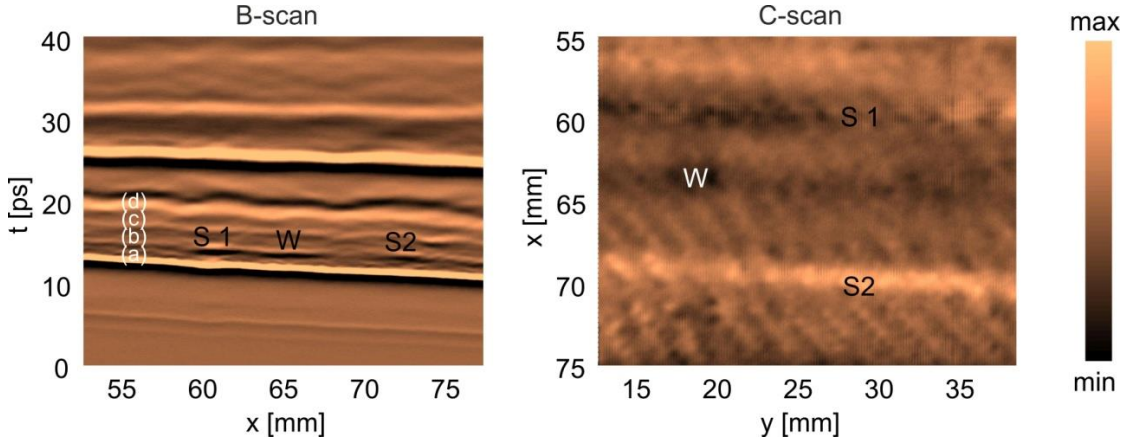

Fig. 6 B-scan and C-scan presenting localisation of the water drop intrusion (W) and two fibre optics with FBG sensors (S1, S2): (a)-(d) – composite layers (Mieloszyk *et al.* 2017)

The water parameters values are presented in a form of complex refractive index (N_W) according to results achieved by Bertie and Lan (1996). It is equal to

$$N_W = n_W + i\kappa_W$$
$$n_W = 2.4 \quad (1)$$
$$\kappa_W = 0.81$$

The GFRP parameters were determined experimentally for a frequency range 0-4 THz. It was performed using THz spectrometer part with a special chamber separated from environmental influence. The complex refractive index (N_S) of the sample is equal to

$$N_S = n_S + i\kappa_S$$
$$n_S = 1.69 \quad (2)$$
$$\kappa_S = 0.055$$

The differences between refractive indexes of those two materials (GFRP composite and water) are high enough to allow the THz spectrometry to detect and localize the water drop. The higher value of absorption coefficient for water indicated that the THz wave is more attenuated propagating throughout water than composite material. The main problem in the research presented in the paper is that the water is not in a form of a layer with equal thickness but because it was embedded in composite material its thickness vary.

B-scan and C-scan of the sample part are presented in Fig. 6. The B-scan allows to count the sample layers as well as determine the location of the water drop and two fibre optics between 1st and 2nd layer. It shows differences in THz wave interaction with two embedded objects. Fibre optics occurrence mostly results in THz wave scattering on their circular cross section. The material parameters of fibre optics and glass fibres in textiles are similar. The embedded ones also locally influenced on shapes of textile layers. The influence is visible on layers above the fibre optics according to the staking sequence during manufacturing procedure. On the other hand, as it was described above, water mostly results in waves attenuation up to its total disappearance. The B-scan also allows to determine the thickness of all presented elements. It can be observed that the water drop disturbance thickness is about two times smaller than the fibre optics which diameter is equal to 250 µm. Roughly it can be written that the drop thickness is similar to the distance between 1st and 2nd layer, because during the manufacturing process the glass material behave like limitation.

C-scan (Fig. 6) was performed for the beginning of the 2nd layer. In the image both fibre optics are visible although their colours differ. One of them is dark while the second is a bright one. The embedded water is visible as a dark circular area with a diameter comparable to the thickness of fibre optics trace. So it allows to determine the water inclusion shape and size on the particular cross-section. Due to high surface tension of water probably the embedded inclusion is in a form of a drop, so its size vary in the sample thickness direction. On the other hand the contaminated (wet) area can be wider if the part with a mixture of water end resin will be also taken into consideration.

The analysed sample is not ideally flat. So C-scans made for one chosen optical delay do not have to show all elements with exact the same distance to the sample's surface – see Fig. 6. Due to this a simple filtering method was proposed. For every signal the first maximum location was determined creating a set of time values related to reflection of THz waves on the sample's surface. This method minimise the influence of the surface roughness and sample curvature.

As the analysed sample is a laminate the consecutive layers are parallel and have similar thickness. The only difference can be an amount of resin between glass fibre textile plies. So a sequence of C-scans presenting internal structure of the sample for chosen time distances between sample's surface were calculated. The present investigation is concerned on the water inclusion between 1st and 2nd layer. Due to this a sequence of four filtered C-scans was calculated – see Fig. 7. The images were determined for time delay (0.686 ps) related to equal division of time range between points W_1 and W_4 (Fig. 5(b)).

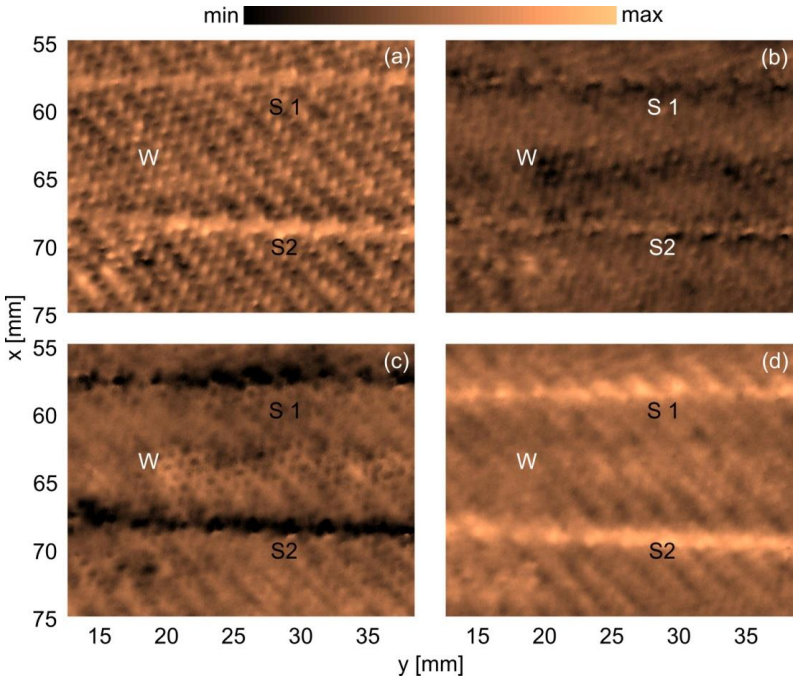

Fig. 7 Sequence of C-scans for time step equal to 0.686 ps

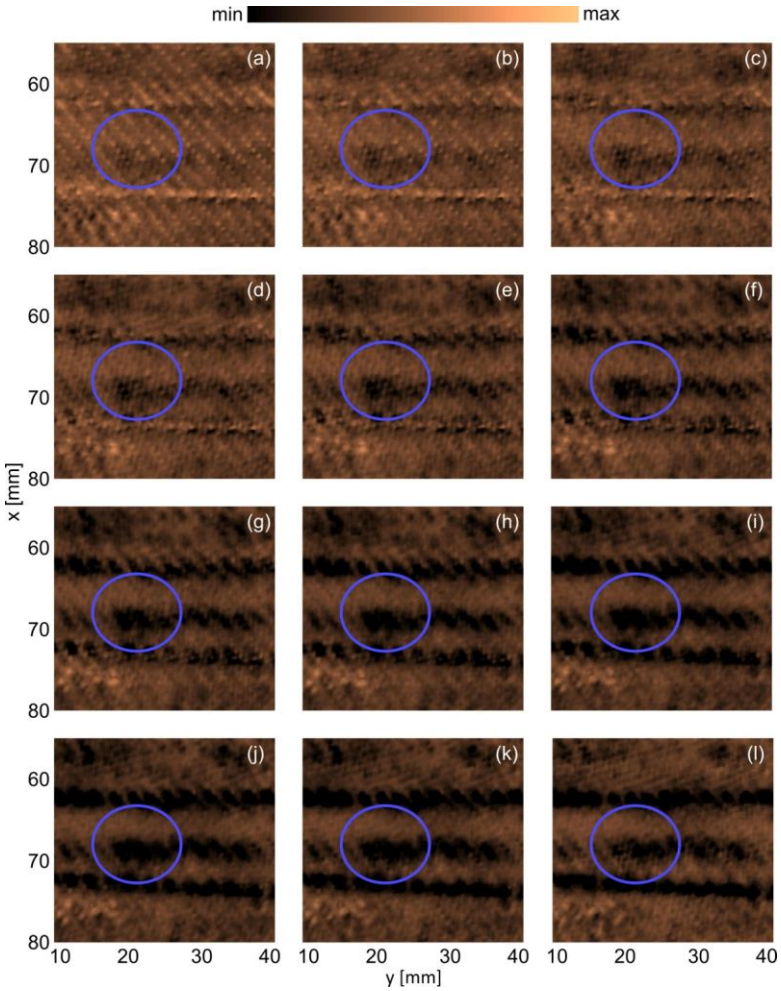

Fig. 8 Sequence of filtered C-scans for time step equal to 0.05 ps

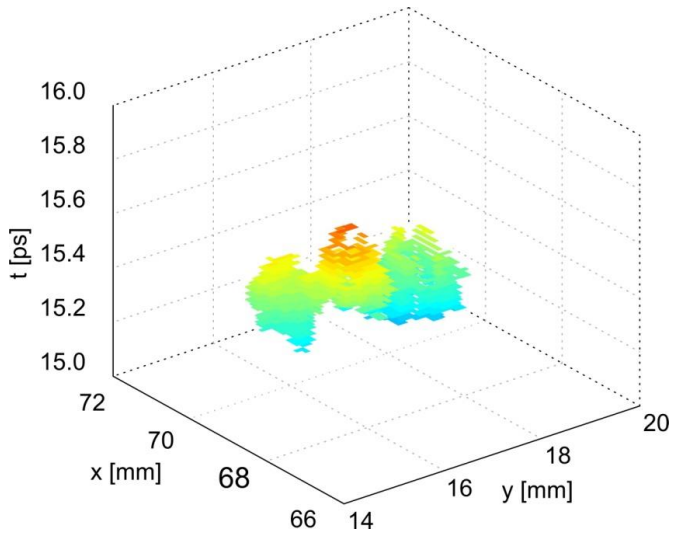

Fig. 9 3-D image of the water drop inclusion (Mieloszyk *et al.* 2017)

All of C-scans show two fibre optics. Their observable influence on THz waves differ in thickness direction and they are visible as bright or dark lines. For the first C-scan (Fig. 7(a)) majority of the THz waves that are reflected from the fibre optics reached the receiver head. While in the second (Fig. 7(b)) the scattering process on the rounded cross size of the fibres results in variety of the reflected rays directions and only a strongly limited part of them reached the receiver. In every image the water inclusion location is marked as 'W' but it is visible in two C-scans only – see Figs. 7(b) and 7(c). It is confirmed that water influence is very local and is not noticed on C-scans made for time before and after the moment when THz wave propagates throughout the water area. This behaviour confirm the local influence of water inclusion.

The embedded water influence is observed in Fig. 5(b) as peak attenuation in time between points denoted as W_2 and W_3. To analyse the changes in the shape of the water drop in time a sequence of filtered C-scans for this time range was calculated. They are presented in Fig. 8. For every image the area with possible influence of water is marked by blue ellipse. The water drop is visible as a dark mark (local minimum) in bright surrounding area. As it is visible the water drop size vary in the thickness direction. On the other side the possibility of the water indication in C-scans is strongly limited by inaccuracy of the sample preparation as well as fibre optics influence. In the first group of C-scans (Figs. 8(a)-8(f)) fibre optics are observed as bright lines or lines with bright and dark pattern. Also water inclusion is well visible as darker area. The situation for the last group of C-scans (Figs. 8(g)-8(l)) differ and fibre optics, water and unequal distribution of resin gives similar response.

The water inclusion is visible on C-scans (Fig. 8) as a local minimum with different shape. The maximum size of the inclusion is 2.5 mm x 5 mm. This characteristic interaction between THz wave and water embedded in composite material allows to propose a filtering method. It is based on differences observed on the THz wave as the local maximum attenuation visible in waveform of wave propagated throughout water inclusion in a time range W_2-W_3 in Fig 5(b). In the analysed case the water drop was embedded between two fibre optics so the filtering process was limited to this area only. The filtering method based on comparison of signal amplitudes measured in every point in the analysed area with this for intact material (denoted as M_1 in Fig. 5) in a range of time: W_2-W_3. For better accuracy of the method for all signals the first maxima were determined and times referred to them were treated as a t = 0. So the sample roughness and its curvature influences were minimised.

4. Conclusions

The paper presents an application of THz spectroscopy method for detection, localisation and determination of size of the water drop intrusion as well as two embedded fibre optics. The contamination was introduced into glass composite sample during its manufacturing process. The proposed method implemented phenomenon of strong attenuation of THz wave during propagation throughout water in contrary with glass composite material. Despite the fact that in the analysed case due to small amount of water its influence was strongly limited it was possible to determine its location between the 1st and the 2nd layer. Additionally two filtering methods were proposed. The first one minimises the sample curvature and allows to precisely determine location of all embedded objects (fibre optics, water drop) influence on surrounding material. While the second allows to remove the surrounding material influence and determine the intrusion shape.

Acknowledgments

The research in this paper was partially supported by the project entitled Reliable and Autonomous Monitoring System for Maritime Structures (MARTECII/RAMMS/1/2016)

granted by National Centre for Research and Development in Poland.

References

Alizadeh, E. and Dehestani, M. (2015), "Analysis of composite girders with hybrid GFRP hat-shape sections and concrete slab", *Struct. Eng. Mech.*, **54**(6), 1135-1152.

Ansari, M.M. and Chakrabartia, A. (2016), "Behaviour of GFRP composite plate under ballistic impact: experimental and FE analyses", *Struct. Eng. Mech.*, **60**(5), 829-849.

Balbekin, N.S., Novoselov, E.V., Pavlov, P.V., Bespalov, V.G. and Petrov, N.V. (2015), "Nondestructive monitoring of aircraft composites using terahertz radiation", *Proceedings of the International Society for Optics and Photonics*, Saratov, Russia.

Baldacci, L., Pagano, M., Masini, L., Toncelli, A., Carelli, G., Storchi, P. and Tredicucci, A. (2017), "Non-invasive absolute measurement of leaf water content using terahertz quantum cascade lasers", *Plant Methods*, **13**, 7pp.

Beldjelili, Y., Tounsi, A. and Mahmoud, S.R. (2016), "Hygro-thermo-mechanical bending of S-FGM plates resting on variable elastic foundations using a four-variable trigonometric plate theory", *Smart Struct. Syst.*, **18**(4), 755-786.

Bertie, J.E. and Lan, Z. (1996), "Infrared intensities of liquids XX: the intensity of the OH stretching band of liquid water revisited, and the best current values of the optical constants of H_2O(I) at 25℃ between 15,000 and 1 cm^{-1}", *Appl. Spectrosc.*, **50**(8), 1047-57.

Budhe, S., Banea, M.D., de Barros, S. and da Silva, L.F.M. (2017), "An updated review of adhesively bonded joints in composite materials", *Int. J. Adhesion Adhesives*, **72**, 30-42.

Cai, Y., Brener, I., Lopata, J., Wynn, J., Pfeiffer, L. and Federici, J. (1997), "Design and performance of singular electric field terahertz photoconducting antennas", *Appl. Phys. Lett.*, **71**, 276-278.

Chaichanawong, J., Thongchuea, C. and Areerat, S. (2016), "Effect of moisture on the mechanical properties of glass fiber reinforced polyamide composites", *Adv. Powder Technol.*, **27**, 898-902.

Chan, W.L., Deibel, J. and Mittleman, D.M. (2007), "Imaging with terahertz radiation", *Reports on progress in physics*, **70**, 13-25.

Ciminello, M., Ameduri, S., Concilio, A., Flauto, D. and Mennella, F. (2015), "Hinge rotation of a morphing rib using FBG strain sensors", *Smart Struct. Syst.*, **15**(6), 1393-1410.

Dong, J., Kim, B., Locquet, A., McKeon, P., Declercq, N. and Citrin, D.S. (2016), "Enhanced terahertz imaging of small forced delamination in woven glass fibre-reinforced composites with wavelet de-noising", *J. Infrared. Millim Te*, **37**, 289-301.

Eftekhari, M. and Fatemi, A. (2016), "Tensile behavior of thermoplastic composites including temperature, moisture, and hygrothermal effects", *Polym. Test*, **51**, 151-164.

Federici, J.F. (2012), "Review of moisture and liquid detection and mapping using terahertz imaging", *J. Infrared Millim Te*, **33**, 97-126.

Fifo, O., Ryan, K. and Basu, B. (2015), "Application of self-healing technique to fibre reinforced polymer wind turbine blade", *Smart Struct. Syst.*, **16**(4), 593-606.

Hajrya, R. and Mechbal, N. (2015), "Perturbation analysis for robust damage detection with application to multifunctional aircraft structures", *Smart Struct. Syst.*, **16**(3), 435-457.

Jung, B.J., Park, J.W., Sim, S.H. and Yi, J.H. (2015), "Issues in structural health monitoring for fixed-type offshore structures under harsh tidal environments", *Smart Struct. Syst.*, **15**(2), 335-353.

Kim, H., Kang, D. and Kim, D.H. (2017), "Mechanical strength of FBG sensor exposed to cyclic thermal load for structural health monitoring", *Smart Struct. Syst.*, **19**(3), 335-340.

Lecheb, S., Nour, A., Chellil, A., Mechakra, H., Ghanem, H. and Kebir, H. (2015), "Dynamic prediction fatigue life of composite wind turbine blade", *Steel Compos. Struct.*, **18**(3), 673-691.

Li, H., Ou, J., Zhang, X., Pei, M. and Li, N. (2015), "Research and practice of health monitoring for long-span bridges in the mainland of China", *Smart Struct. Syst.*, **15**(3), 555-576.

Majewska, K., Mieloszyk, M. and Ostachowicz, W. (2016), "Glass fibre composite elements with embedded fibre Bragg grating sensors inspected by thermography techniques", *Proceedings of the EWSHM*, Bilbao Spain.

Malekzadeh, M., Gul, M., Kwon, I.B. and Catbas, N. (2014), "An integrated approach for structural health monitoring using an in-house built fiber optic system and non-parametric data analysis", *Smart Struct. Syst.*, **14**(5), 917-942.

Malinowski, P., Pałka, N., Opoka, S., Wandowski, T. and Ostachowicz, W. (2015), "Moisture detection in composites by terahertz spectroscopy", *J. Phy. Conf. Series*, **628**, 012100 (8).

Mieloszyk, M., Majewska, K. and Ostachowicz, W. (2017a), "Detection and localisation of water intrusion in glass fibre reinforced composite using THz spectroscopy", *Proceedings of the SMART 2017*, Madrid, Spain.

Mittleman, D. (2003), *Sensing with Terahertz Radiation*, Springer-Verlag Berlin Heidelberg, Germany.

Miyamoto, A. and Motoshita, M. (2017), "An Intelligent bridge with an advanced monitoring system and smart control techniques", *Smart Struct. Syst.*, **19**(6), 587-599.

Numan, H.A., Tayşi, N. and Ö zakca, M. (2016), "Experimental and finite element parametric investigations of the thermal behavior of CBGB", *Steel Compos. Struct.*, **20**(4), 813-832.

Park, C., Park, Y., Kim, S. and Ju, M. (2016), "New emerging surface treatment of hybrid GFRP bar for stronger durability of concrete structures", *Smart Struct. Syst.*, **17**(4), 593-610.

Radzieński, M., Mieloszyk, M., Rahani, E.K., Kundu, T. and Ostachowicz, W. (2015), "Heat induced damage detection in composite materials by terahertz radiation", *Proceedings of the SPIE Smart Structures and Materials+ Nondestructive Evaluation and Health Monitoring*, Portland, USA.

Ryu, C.H., Park, S.H., Kim, D.H., Jhang, K.Y. and Kim, H.S. (2016), "Nondestructive evaluation of hidden multi-delamination in a glass-fiber-reinforced plastic composite using terahertz spectroscopy", *Compos. Struct.*, **156**, 338-347.

Sarkar, K. and Bhattacharjee, B. (2014), "Moisture distribution in concrete subjected to rain induced wetting-drying", *Comput. Concrete*, **14**(6), 635-656.

Sung, H.J., Do, T.M., Kim, J.M. and Kim, Y.S. (2017), "Long-term monitoring of ground anchor tensile forces by FBG sensors embedded tendon", *Smart Struct. Syst.*, **19**(3), 269-277.

Teng, J., Lu, W., Wen, R. and Zhang, T. (2015), "Instrumentation on structural health monitoring systems to real world structures", *Smart Struct. Syst.*, **15**(1), 151-167.

Wang, G., Pran, K., Sagvolden, G., Havsgard, G.B., Jensen, A.E., Johnson, G.A. and Vohra, S.T. (2001), "Ship hull structure monitoring using fibre optic sensors", *Smart Mater Struct.*, **10**, 472-478.

Wang, H., Tao, T., Li, A. and Zhang, Y. (2016), "Structural health monitoring system for Sutong Cable-stayed Bridge", *Smart Struct. Syst.*, **18**(2), 317-334.

Xin, H., Liu, Y. and Du, A. (2015), "Thermal analysis on composite girder with hybrid GFRP-concrete deck", *Steel Compos. Struct.*, **19**(5), 1221-1236.

Xu, Y.L., Huang, Q., Xia, Y. and Liu, H.J. (2015), "Integration of health monitoring and vibration control for smart building structures with time-varying structural parameters and unknown excitations", *Smart Struct. Syst.*, **15**(3), 807-830.

Zhang, Q., Xia, Q., Zhang, J. and Wu, Z. (2016), "Optimal layout of long-gauge sensors for deformation distribution identification", *Smart Struct. Syst.*, **18**(3), 389-403.

Zhang, W., Tong, F., Gu, X. and Xi, Y. (2015), "Study on moisture transport in concrete in atmospheric environment", *Comput. Concrete*, **16**(5), 775-793.

Zhou, H.F., Ni, Y.Q. and Ko, J.M. (2013), "Structural health monitoring of the Jiangyin Bridge: system upgrade and data analysis", *Smart Struct. Syst.*, **11**(6), 637-662.